CHARACTERISTICS OF THE SHELL-TYPE CORIOLIS FLOWMETER

J. KUTIN AND I. BAJSIĆ

Laboratory of Measurements in Process Engineering, Faculty of Mechanical Engineering, University of Ljubljana, Aškerčeva 6, Ljubljana 1000, Slovenia

The primary element of the Coriolis flowmeter is a measuring tube conveying fluid. While the tube in the classical meter undergoes a beam-type vibration, the shell-type tube vibrates in the second circumferential mode. This paper analyzes theoretical characteristics of the straight-tube shell-type Coriolis meter. A mathematical model founded on the theory of Flügge thin shell and linearized potential flow was used. The results show the similarity between measuring principles in the shell-type and the beam-type meter. Finally, we carried out a comparison with the straight-tube beam-type meter, based on the condition that both meters have the same pressure loss. It was found that the shell-type meter has a higher working frequency and a larger phase shift due to flow.

© 1999 Academic Press

1. INTRODUCTION

In the Coriolis flowmeter, fluid flows through a measuring tube, clamped at both ends. Under the influence of a harmonic exciting force in the proper control system (e.g., phase-locked loop), the tube performs a harmonic vibration at its resonant frequency. The fluid flow causes an alteration of the fundamental mode shape and natural frequency of the tube. Using motion sensors and processing electronics, the tube is utilized as a mass flowrate and fluid density measuring device.

The measuring tube is usually slender and vibrates in the lateral (first circumferential, beam-type) mode. Figure 1(a) shows this kind of mode shape for the straight tube. There are many scientific articles discussing the physical phenomena and theoretical characteristics of the so-called beam-type Coriolis meter. Sultan and Hemp [1] presented the mathematical model of the straight-tube and U-tube configurations, based on the theory of Euler beam and one-dimensional fluid flow. References [2–4] examined the nature and limitations of the meter's ideal characteristics using the theory of small perturbations. Subsequent work has been focused on a mathematical model extension, e.g., by introducing the added-masses effect of the exciter [5] and motion sensors [6]. A particular analysis is presented by the weight vector theory, which can also deal with the velocity distribution effects in the flowmeter [7–9].
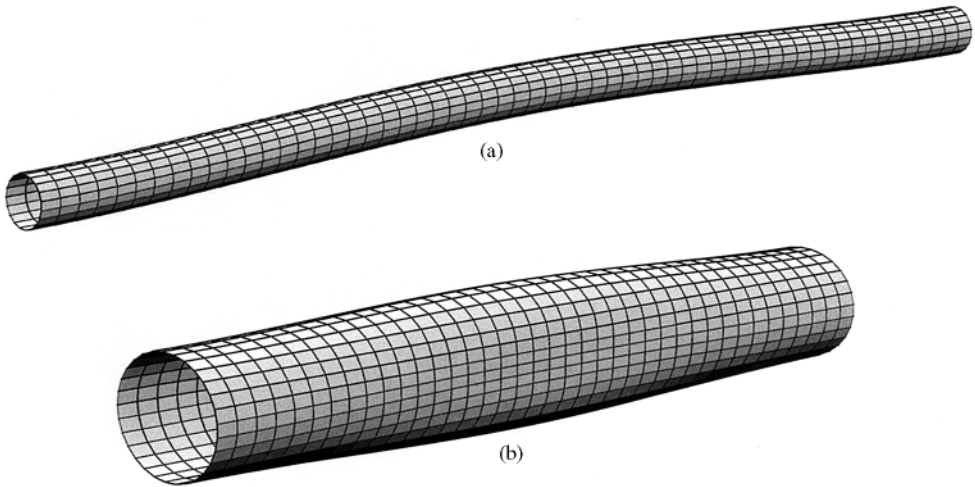
Figure 1. Mode shapes of the straight measuring tube: (a) beam-type and (b) shell-type Coriolis meter.

In this paper, the so-called shell-type Coriolis flowmeter is analyzed [10, 11]. Its straight measuring tube experiences a second circumferential (shell-type) vibration mode (Figure 1(b)). The mathematical model used to describe the shell-type meter is based on the theory of flow-induced vibrations [12–14]. One of the topics of this scientific area also investigates the stability of thin-walled tubes (cylindrical shells) conveying fluid; the review of corresponding literature is given in references [13, 14]. Although the scope of the flow-induced vibration area mostly deviates from the purpose of flow measurement, the required theory is identical for determining both the stability limits and the basic measuring effects. In the paper, Flügge thin shell and linearized potential flow theories are used to describe the measuring tube motion and the measured fluid flow respectively. Our intention is to present basic theoretical characteristics of the mass flowrate and fluid density measurement with the straight-tube shell-type Coriolis meter. In order to estimate its quality, a comparison with the straight-tube beam-type meter is also made.

2. MATHEMATICAL MODEL

2.1. BASIC ASSUMPTIONS

The measuring tube is a straight, circular cylindrical shell, clamped at both ends. Its geometry is defined by its length L, wall thickness h and middle-surface radius R (Figure 2), and its material properties are density ρ_t, the Poisson ratio μ and modulus of elasticity E. Tube deflections are small enough thus allowing the linear, elastic shell theory to be used [15, 16]. The tube wall is sufficiently thin (h^2/R^2 is small compared to unity) for Flügge's version of the equation of motion to be adequate. The added-mass effect of the exciters and motion sensors is neglected. It is assumed that the tube vibration damping is small enough for the model with undamped free motion to be used to obtain the desired results.
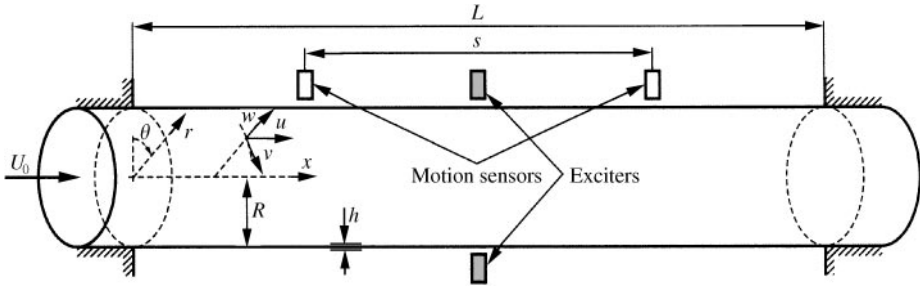
Figure 2. Model of the shell-type Coriolis meter.

The fluid flow to be measured is incompressible (fluid density ρ_0 is constant). It will be characterized by means of potential flow theory, thus, it is considered to be inviscid and irrotational. In the absence of tube vibration, the flow is steady and is defined by its uniform velocity U_0 in x direction (Figure 2) and static pressure P_0. It is assumed that flow field disturbances, caused by tube vibration, are sufficiently small compared to the undisturbed flow. Therefore, the linearized (first order) potential flow theory [17] could be used in order to describe the influence of flow on tube vibration.

2.2. EQUATIONS OF MOTION AND BOUNDARY CONDITIONS

The shell-tube deflections can be described by axial, circumferential and radial middle-surface displacements (u, v, w) in the directions of the cylindrical polar co-ordinates (x, θ, r) (Figure 2). The Flügge's equations of motion for a circular cylindrical shell [15] could be written in a symbolic notation as

$$L_{11}u + L_{12}v + L_{13}w = \frac{\partial^2 u}{\partial t^2}, \quad L_{21}u + L_{22}v + L_{23}w = \frac{\partial^2 v}{\partial t^2},$$

$$L_{31}u + L_{32}v + L_{33}w = -\frac{\partial^2 w}{\partial t^2} + \frac{R_i}{R}\frac{P_i}{h\rho_t}, \tag{1}$$

where L_{ij} are linear differential operators (appendix), R_i is the tube internal-surface radius and P_i is the fluid pressure on the internal surface. The operators L_{ij} include partial derivatives with respect to x and θ and tube geometrical and material parameters. The quotient R_i/R in equation (1) represents the ratio between the area of the tube internal and middle-surface. For clamped ends, the tube boundary conditions are given by

$$u = v = w = \frac{\partial w}{\partial x} = 0 \quad \text{at } x = 0, \quad x = L. \tag{2}$$

The fluid–tube interaction is given by the fluid pressure P_i, which may be determined by the unsteady Bernoulli equation:

$$\frac{\partial \Phi}{\partial t} + \frac{V^2}{2} + \frac{P}{\rho_0} = \text{constant}, \tag{3}$$

where Φ is the velocity potential, V is the magnitude of the velocity vector $\mathbf{V} = (V_x, V_\theta, V_r)$ and P is the pressure in the perturbed flow field. The relation between the velocity field and the velocity potential is

$$\mathbf{V} = \mathbf{\nabla}\Phi \quad \text{or} \quad V_x = U_0 + \frac{\partial\varphi}{\partial x}, \quad V_\theta = \frac{1}{r}\frac{\partial\varphi}{\partial\theta}, \quad V_r = \frac{\partial\phi}{\partial r}, \tag{4}$$

where Φ is considered to consist of the undisturbed component $U_0 x$ and the perturbation velocity potential φ. Expressing the pressure in the similar way, $P = P_0 + p$, and neglecting second order perturbations in equation (3), the fluid pressure on the internal surface of the tube is

$$P_i = P_0 + p_i = P_0 - \rho_0\left(\frac{\partial\varphi}{\partial t} + U_0\frac{\partial\varphi}{\partial x}\right)\Bigg|_{r = R_i}. \tag{5}$$

The static effect of the pressure P_0 exceeds the scope of our paper. Therefore, the fluid–tube interaction is only the consequence of the tube vibration ($P_i \equiv p_i$). Using equation (4) and the continuity equation of the incompressible fluid flow, $\mathbf{\nabla}\cdot\mathbf{V} = 0$, leads to the Laplace equation for perturbation velocity potential φ:

$$\frac{\partial^2\varphi}{\partial r^2} + \frac{1}{r}\frac{\partial\varphi}{\partial r} + \frac{1}{r^2}\frac{\partial^2\varphi}{\partial\theta^2} + \frac{\partial^2\varphi}{\partial x^2} = 0. \tag{6}$$

A general solution of equation (6) has to satisfy boundary conditions that no fluid passes through the tube surface,

$$\frac{\partial\varphi}{\partial r}\Bigg|_{r = R_i} = \frac{\partial w}{\partial t} + U_0\frac{\partial w}{\partial x} \quad \text{for } 0 \leqslant x \leqslant L, \tag{7}$$

and that the velocity potential remains finite inside the tube.

2.3. SOLUTION PROCEDURE

The solution is obtained by using a procedure, similar to that in reference [18]. The derivation of the fluid pressure does not include the realistic flow conditions at the tube ends, which come after the fact that w is identically zero for $x < 0$ and $x > L$. This simplification may have a considerable influence when L/R is too small (see, for example, references [19–21], where Fourier integral theory and Galerkin's method are used to obtain the solution). For tubes long enough ($L/R \geqslant 10$ for the most part of the paper), these errors could be neglected.

If the shell-tube vibration is periodic circumferentially and harmonic in time, general solutions for axial, circumferential and radial displacement can be expressed in a complex form as

$$u = \sum_j A_j\,\mathrm{e}^{\mathrm{i}\lambda_j x}\cos n\theta\,\mathrm{e}^{\mathrm{i}\omega t}, \quad v = \sum_j B_j\,\mathrm{e}^{\mathrm{i}\lambda_j x}\sin n\theta\,\mathrm{e}^{\mathrm{i}\omega t}, \quad w = \sum_j C_j\,\mathrm{e}^{\mathrm{i}\lambda_j x}\cos n\theta\,\mathrm{e}^{\mathrm{i}\omega t}, \tag{8}$$

and similarly for the perturbation velocity potential as

$$\varphi = \sum_j D_j(r)\, \mathrm{e}^{\mathrm{i}\lambda_j x} \cos n\theta\, \mathrm{e}^{\mathrm{i}\omega t}, \tag{9}$$

where λ_j are the eigenvalues, n is the circumferential wave number and ω is the circular frequency in the range of calculations in this paper, ω is wholly real. By introducing equation (9) into equations (5)–(7), the fluid pressure distribution on the internal tube surface, expressed as the function of the tube motion, is

$$p_i = -\rho_0 \sum_j \frac{I_n(\lambda_j R_i)}{\mathrm{d}I_n(\lambda_j r)/\mathrm{d}r|_{r=R_i}} \left(\frac{\partial^2 w_j}{\partial t^2} + 2U_0 \frac{\partial^2 w_j}{\partial t\,\partial x} + U_0^2 \frac{\partial^2 w_j}{\partial x^2} \right), \tag{10}$$

where $w = \sum_j w_j$ and $I_n(\ )$ is nth order modified Bessel function of the first kind. Term $\partial^2 w_j/\partial t^2$ is a translational acceleration, $2U_0 \partial^2 w_j/\partial t\,\partial x$ is a Coriolis acceleration ($\partial^2 w_j/\partial t\,\partial x$ is a local angular velocity) and $U_0^2 \partial^2 w_j/\partial x^2$ is a centrifugal acceleration ($\partial^2 w_j/\partial x^2$ is a local curvature).

By introducing equation (10) into equation (1), one can proceed to the solution of Flügge's equations. Using the assumed solution for displacements (equation (8)) yields a homogeneous set of three linear equations in A_j, B_j and C_j. For non-trivial solutions, the determinant of the coefficients has to vanish thus yielding a transcendental equation in λ_j. For eight boundary conditions (equation (2)), eight values of λ_j (and eight solutions A_j/C_j, B_j/C_j) are of interest. It is appropriate to choose the eigenvalues with the smallest modulus, because they contribute the most to the formation of the mode shapes [18]. Introducing the boundary conditions (2) yields a homogeneous set of eight linear equations in C_j. Setting the determinant of the coefficients equal to zero, one obtains a transcendental equation in the circular frequency ω. Its mth consecutive positive root is the natural frequency of the vibrating tube with m axial half-waves and n circumferential waves.

The actual displacements and perturbation velocity potential are calculated as the real part of the supposed complex solutions (equations (8) and (9)). The results can be written as follows:

$$u = \bar{u}(x)\cos n\theta \cos(\omega t + \phi_u(x)), \quad v = \bar{v}(x)\sin n\theta \cos(\omega t + \phi_v(x)),$$

$$w = \bar{w}(x)\cos n\theta \cos(\omega t + \phi_w(x)), \quad \varphi = \bar{\varphi}(r,x)\cos n\theta \cos(\omega t + \phi_p(r,x)), \tag{11}$$

where $\bar{u}$, $\bar{v}$, $\bar{w}$, $\bar{\varphi}$ and ϕ_u, ϕ_v, ϕ_w, ϕ_φ are corresponding amplitudes and initial phases respectively. The displacements and velocity potential are normalized according to

$$\int_0^L \bar{w}(x)^2\, \mathrm{d}x = L. \tag{12}$$

The above calculation gives all claimed parameters to analyze free vibration modes of the shell-tube with the internal fluid flow: the natural frequency and the mode shapes. Therefore, one can use this model to characterize the behaviour of the shell-type Coriolis meter.

3. METER CHARACTERISTICS

The Coriolis meter is used to measure the mass flowrate $q_m = U_0\rho_0\pi R_i^2$ and fluid density ρ_0. This paper deals with the shell-type Coriolis meter whose tube vibration models composed of two circumferential waves ($n = 2$) and one axial half-wave ($m = 1$). Its measuring effect is obtained from signals of two motion sensors, which detect the tube vibration in a radial direction. The sensors are located symmetrically with regard to the midpoint of the tube length. Therefore, their axial positions could be given as $x_1 = (L - s)/2$ and $x_2 = (L + s)/2$, where s is the distance between the sensors (Figure 2). With the intention of attaining the largest radial mode amplitude, the most appropriate measuring plane (rx plane) in the circumferential direction is at $\theta_1 = \theta_2 = k\pi/2$, where k is any integer.

Figure 3 shows the time dependence of the axial and radial displacement, u and w, (the circumferential displacement v is zero here) in the measuring plane for selected input data. Due to the relative small effect of the axial mode, the phase and time difference between signals from the sensors, $\Delta\phi$ and Δt, can be determined as

$$\Delta\phi = \phi_w(x_2) - \phi_w(x_1), \quad \Delta t = \Delta\phi/\omega. \tag{13}$$

If there is no fluid flowing inside the tube, the phase difference is zero (Figure 3(a)). However, the Coriolis force, caused by fluid flow, makes an asymmetrical alteration in the basic mode shape: the radial motion of the tube inlet lags behind the outlet one (Figure 3(b)). Figure 4 shows the tube cross-section in the measuring plane and the isopotential lines of the perturbed fluid flow at the moment $\omega t = \pi/4$. Its comparison with the tube radial mode in Figure 3 highlights the interaction between the vibrating tube and internal fluid flow.
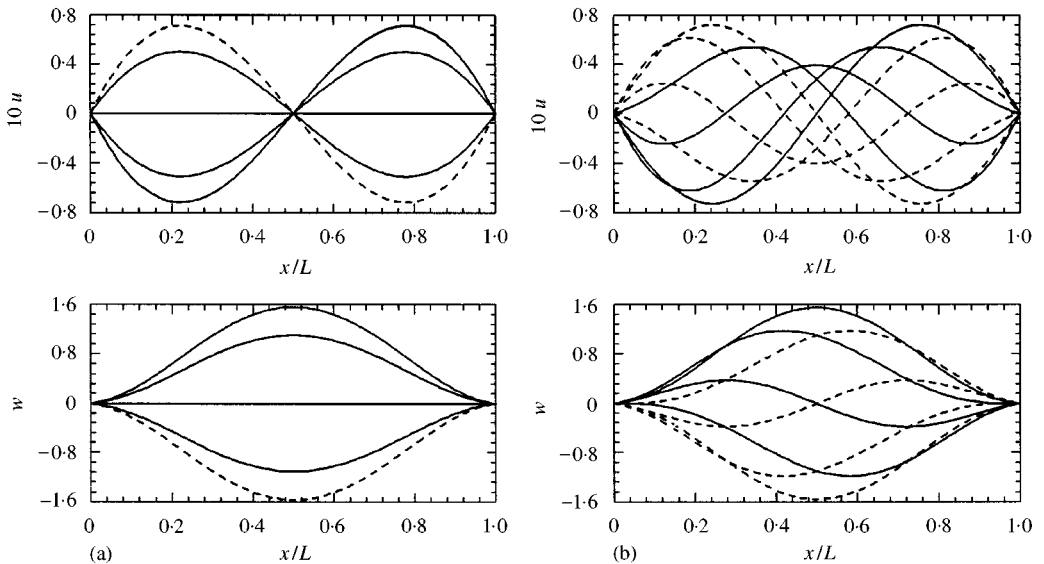

Figure 3. Time dependence of axial and radial tube deflection, u and w, at $\theta = 0$, circumferential deflection v is zero ($m = 1$, $n = 2$, $\rho_0 = 1000$ kg/m³, $L = 0.15$ m, $R = 10$ mm, $h = 0.5$ mm, $\mu = 0.3$, $\rho_t = 4500$ kg/m³, $E = 110$ GN/m²): (a) quiescent fluid; (b) flowing fluid, $q_m = 50$ kg/s.

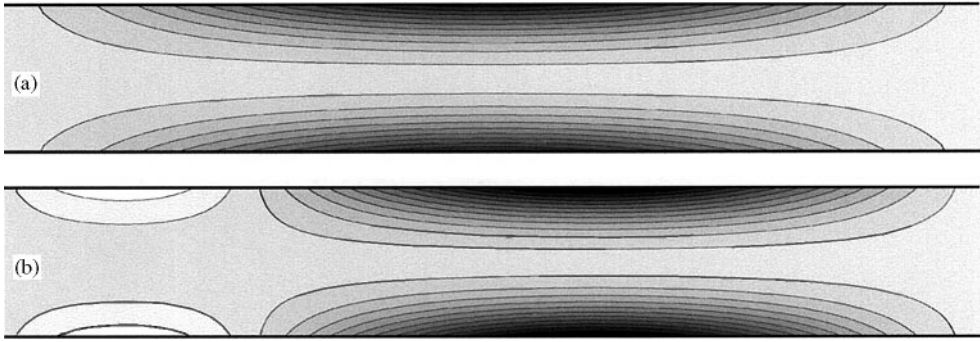Figure 4. Perturbation velocity isopotential lines in the cross-section of the vibrating tube at $\theta = 0$, π and $\omega t = \pi/4$ (data as in Figure 3): (a) quiescent fluid; (b) flowing fluid, $q_m = 50$ kg/s. 14 contours between -95 and 20 m^2/s (shading from black to white).
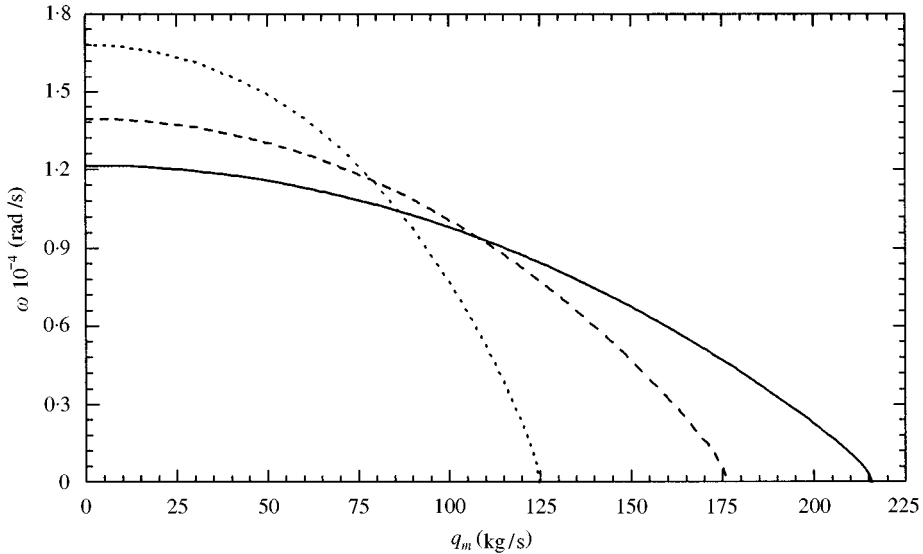

Figure 5. Variation of the natural frequency with the mass flowrate for three values of the fluid density (other data as in Figure 3): ———, $\rho_0 = 1500$ kg/m^3; - - -, $\rho_0 = 1000$ kg/m^3; $\cdots\cdots$, $\rho_0 = 500$ kg/m^3.

Figures 5 and 6 show the fluid flow effect on the natural frequency and the phase difference, respectively, for the selected input data. The flow range represents the stable, under-critical region of the vibrating system. Over the critical mass flowrate $q_{m,cr}$, static instability (also called buckling or divergence [14]) occurs: the natural frequency vanishes and negative vibrational damping (amplification of vibration) occurs. In the given example, the mode shape at the critical flowrate has a similar form to the mode shape for $m = 2$ at the zero flow ($\Delta\varphi_{cr} = \pi$). The behaviour can be changed for other input data, e.g., for different tube length (Figure 7). A denotation m_{cr} is used for the number of axial half-waves at the critical flowrate.
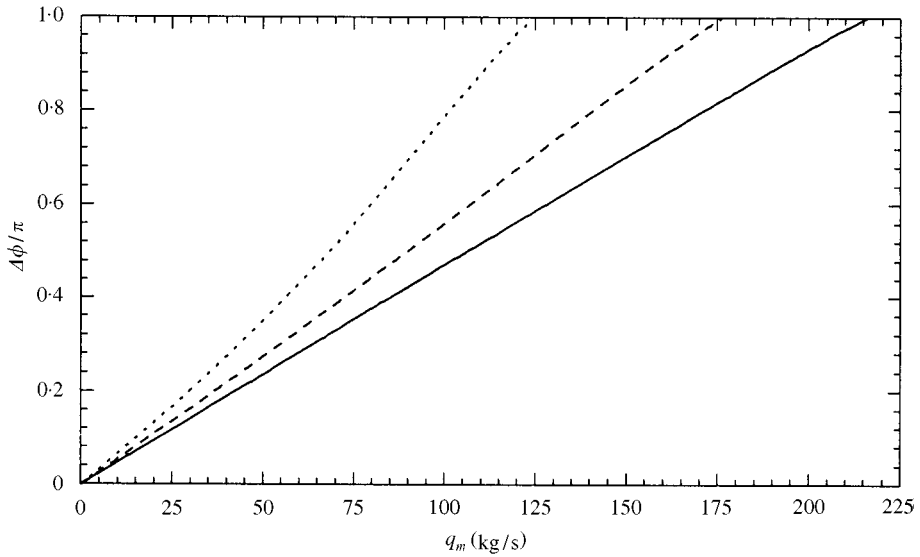
Figure 6. Variation of the relative phase difference with the mass flowrate for three values of the fluid density ($s/L = 0.5$, other data as in Figure 3): ——, $\rho_0 = 1500$ kg/m^3; - - -, $\rho_0 = 1000$ kg/m^3; $\cdots\cdots$, $\rho_0 = 500$ kg/m^3.

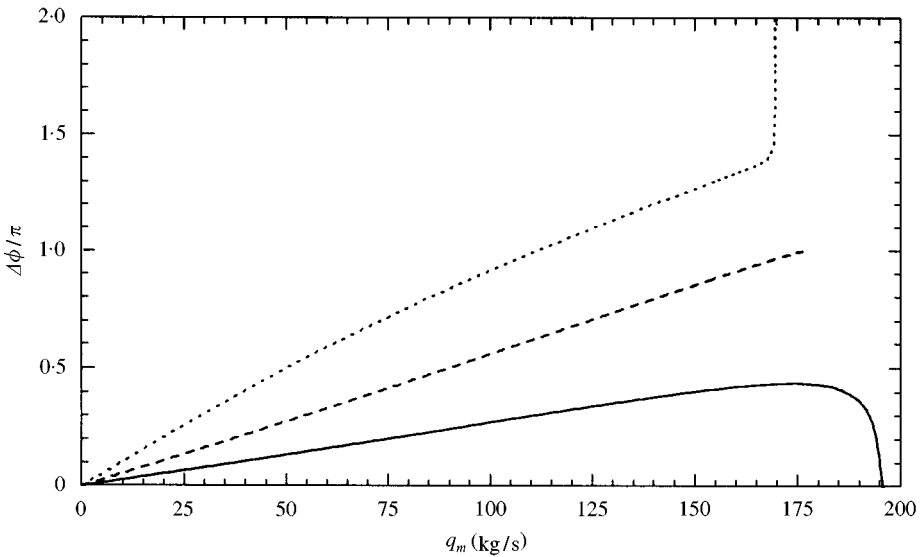

Figure 7. Variation of the relative phase difference with the mass flowrate for three values of the tube length ($s/L = 0.5$, other data as in Figure 3): ——, $L = 0.1$ m ($m_{cr} = 1$); - - -, $L = 0.15$ m ($m_{cr} = 2$); $\cdots\cdots$, $L = 0.2$ m ($m_{cr} = 3$).

Approaching the stability limit leads to intensive alteration of the system characteristics. For sufficiently small flowrates, linear dependence between the phase difference and mass flowrate could be seen (Figures 6 and 7). If the time difference is used instead of the phase difference, a small fluid density effect can be

achieved (Figure 8). Results of this kind allow the time difference to be used for mass flowrate measurement in the Coriolis meter.

   In contrast to the time difference, the natural frequency varies significantly with fluid density and is little effected by sufficiently small flowrates (Figures 5 and 9).
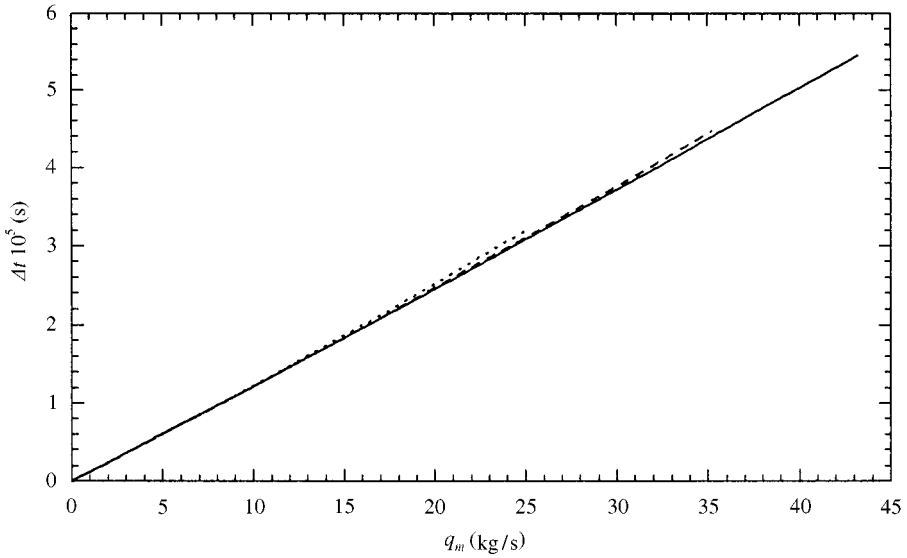

Figure 8. Variation of the time difference with the mass flowrate for three values of the fluid density ($s/L = 0\cdot5$, other data as in Figure 3): ——, $\rho_0 = 1500$ kg/m^3; - - -, $\rho_0 = 1000$ kg/m^3; $\cdots$, $\rho_0 = 500$ kg/m^3.

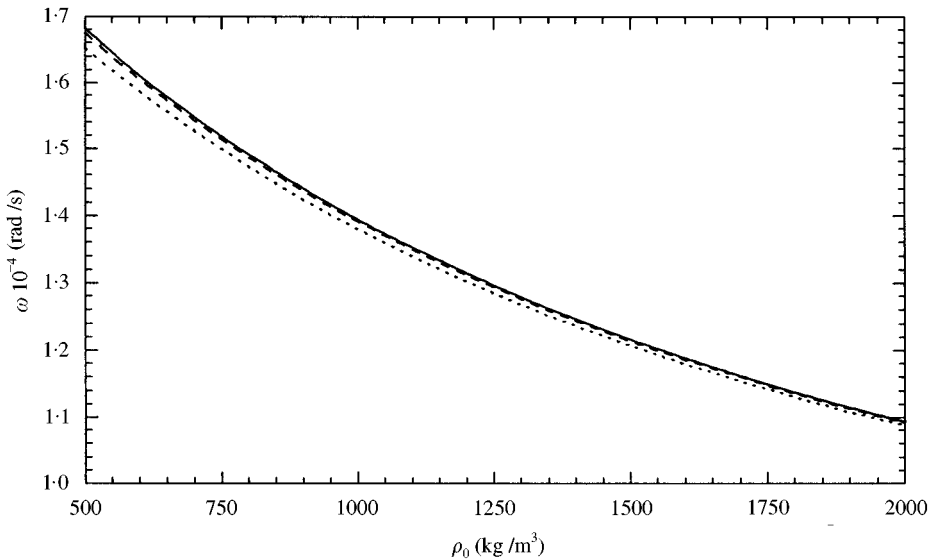
Figure 9. Variation of the natural frequency with the fluid density for three values of the mass flowrate (other data as in Figure 3): ——, $q_m = 0$ kg/s; - - -, $q_m = 10$ kg/s; $\cdots$, $q_m = 20$ kg/s.

The characteristic is non-linear, but it is appropriate to use the alterations in natural frequency for fluid density measurement.

The above discussion shows that the measuring characteristics of the shell-type Coriolis meter are similar to those of the beam-type meter (see, e.g., references [1–3]). Therefore, one could expect an identical condition for the preservation of the ideal meter characteristics (independence of the mass flowrate and fluid density measurement, linear dependence between the phase or time difference and mass flowrate), that is $q_m^2 \ll q_{m,cr}^2$ [2].

4. COMPARISON BETWEEN THE SHELL-TYPE AND THE BEAM-TYPE METER

Relatively small sensitivity and large pressure drop are two of the most negative characteristics of the Coriolis meter. The magnitude of measurable phase difference (measurable with appropriate precision) defines the lower limit of the flowrate measuring range. However, the upper mass flowrate is limited by the admissible pressure drop and independence of mass flowrate and fluid density measurement. Therefore, producers try to find new meter configurations, some of them using curved measuring tubes that enable a larger ratio between the measuring effect and pressure loss. However, the straight-tube meters have some significant advantages: wider dynamic range (i.e., the frequency range without the resonant effects), simple construction and smaller dimensions. In this section, we compare the characteristics of the shell-type ($n = 2$, $m = 1$) and the beam-type ($n = 1$, $m = 1$) straight-tube Coriolis meter.

4.1. COMPARISON BETWEEN THE MATHEMATICAL MODELS

Before making a comparison between the characteristics of meters, one has to decide what kind of theoretical model will be used to describe the beam-type meter. Its theoretical analyses are mostly based on the theory of Euler beam and one-dimensional fluid flow, e.g. [1–3]. The pertaining equation of the tube lateral motion has a form

$$EI \frac{\partial^4 \tilde{w}}{\partial x^4} + M_t \frac{\partial^2 \tilde{w}}{\partial t^2} + M_0 \left(U_0^2 \frac{\partial^2 \tilde{w}}{\partial x^2} + 2U_0 \frac{\partial^2 \tilde{w}}{\partial x \partial t} + \frac{\partial^2 \tilde{w}}{\partial t^2} \right) = 0 \qquad (14)$$

and the boundary conditions for the clamped–clamped tube are

$$\tilde{w} = \frac{\partial \tilde{w}}{\partial x} = 0 \quad \text{at } x = 0, \quad x = L, \qquad (15)$$

where $\tilde{w}$ is the lateral tube deflection, I is the second moment of tube cross-sectional area about a diameter, M_t and M_0 are the tube and fluid mass per unit length respectively.

Certainly, the beam-type meter could also be dealt with the model shown in section 2 ($n = 1$). Figure 10 shows the variation in natural frequency and phase difference of the first lateral mode with the tube length. For a comparison, the
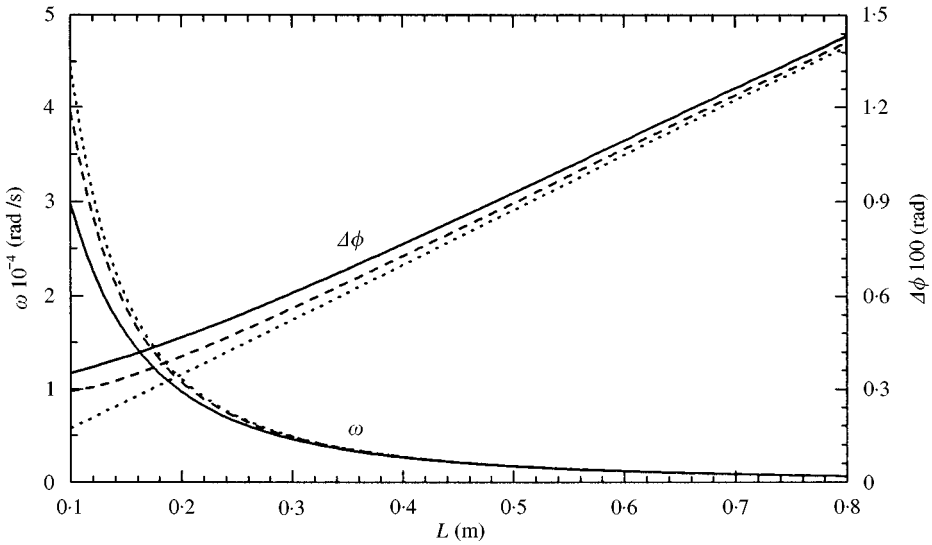
Figure 10. Variation of the natural frequency and phase difference with the tube length for three different mathematical models ($n = 1$, $q_m = 1$ kg/s, $s/L = 0.5$, other data as in Figure 3): ——, Flügge shell theory (8 boundary conditions); - - -, Flügge shell theory (4 boundary conditions); · · · ·, Euler beam theory.

observed parameters were also calculated from Flügge's shell equations with four boundary conditions ($w = \partial w/\partial x = 0$ at both ends, four values of λ_j with the smallest modulus). It is evident that the theory of Euler beam and one-dimensional fluid flow is more appropriate for tubes with a sufficient length ratio L/R. The validity of the beam theory is also conditional on sufficiently large wall thickness ratio h/R. As Flügge shell theory is more general and "exact", the model shown in section 2 is also used for beam-type meter analyses.

4.2. COMPARISON BETWEEN THE METERS

In the comparative analysis of the shell- and the beam-type Coriolis meter, the following basic facts are considered:

(i) *The measuring tube.* The wall thickness ratio h/R is the same for both meters, but the length ratio L/R is generally smaller for the shell-type meter. The meter tubes have the same material properties (ρ_t, E, μ) and absolute roughness ε of the internal surface.

(ii) *The fluid flow to be measured.* For both meters, the same values of mass flowrate q_m and pressure drop ΔP are chosen. The fluid density ρ_0 and kinematic viscosity v_0 are also the same for both meters.

In the calculation of pressure drop through the Coriolis meter, consider only the line losses in the measuring tube. They can be defined as

$$\Delta P = \lambda \frac{L}{D_i} \frac{\rho_0 U_0^2}{2}, \tag{16}$$

where λ is the line loss coefficient and can be determined from the Colebrook–White equation [22]:

$$\frac{1}{\sqrt{\lambda}} = 1{\cdot}74 - 2\log\left(\frac{2\varepsilon}{D_i} + \frac{18{\cdot}7}{\text{Re}\sqrt{\lambda}}\right), \tag{17}$$

where D_i is the tube internal diameter, $D_i = 2R_i$, and Re is the Reynolds number, $\text{Re} = D_i U_0/\nu_0$.

   In the above procedure, the tube dimensions h, R and L could be iteratively calculated for given ratios h/R and L/R and other assumptions. Therefore, we have all the required input data to calculate the natural frequency and phase difference of the measuring system. The described procedure could be an appropriate way to compare the theoretical characteristics of different type Coriolis meters. With equivalent pressure loss, we give assurance of choosing meters with the identical limit of the upper mass flowrate. So the phase difference, determined at that mass flowrate, could be used to compare the sensitivity of meters.

   Figures 11 and 12 show the variation of the natural frequency and the phase difference, respectively, with the tube length ratio for the shell-type ($n = 2$, $m = 1$) and the beam-type ($n = 1$, $m = 1$) Coriolis meter. For both meters, the natural frequency decreases and the phase difference increases with the increasing length ratio. (Although it is not calculated in the paper, it should be known that a similar trend is typical for the decreasing thickness ratio at the constant length ratio.) Generally, the shell-type meter has both observed parameters larger by nearly one order of magnitude. The higher working frequency extends the meter dynamic range and the higher frequency signals are also more suitable for electronic
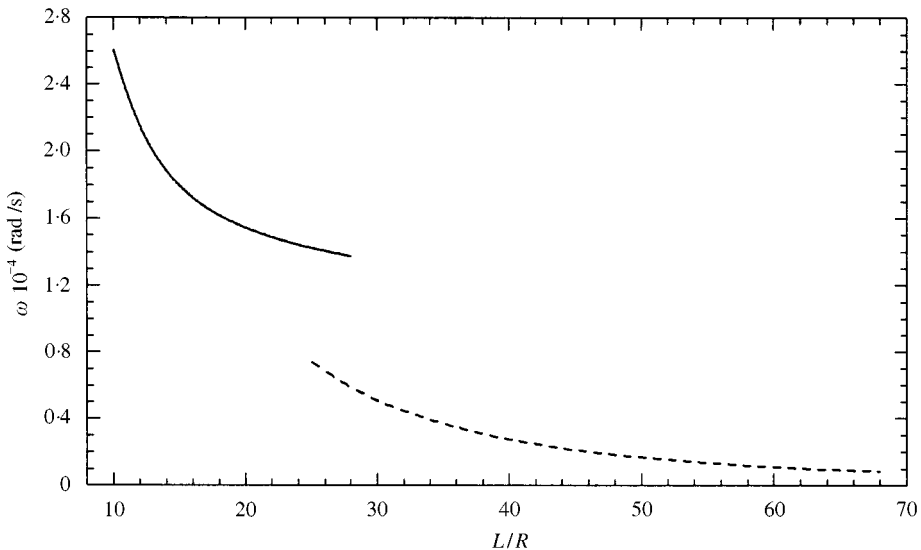

Figure 11. Variation of the natural frequency with the tube length ratio for $n = 2$ and 1 ($m = 1$, $\rho_0 = 1000\ \text{kg/m}^3$, $\nu_0 = 1\ \text{mm}^2/\text{s}$, $\varepsilon = 0{\cdot}01\ \text{mm}$, $q_m = 6\ \text{kg/s}$, $\Delta P = 0{\cdot}4\ \text{bar}$, $h/R = 0{\cdot}05$, $\mu = 0{\cdot}3$, $\rho_t = 4500\ \text{kg/m}^3$, $E = 110\ \text{GN/m}^2$): ——, shell-type meter, $n = 2$; - - -, beam-type meter, $n = 1$.
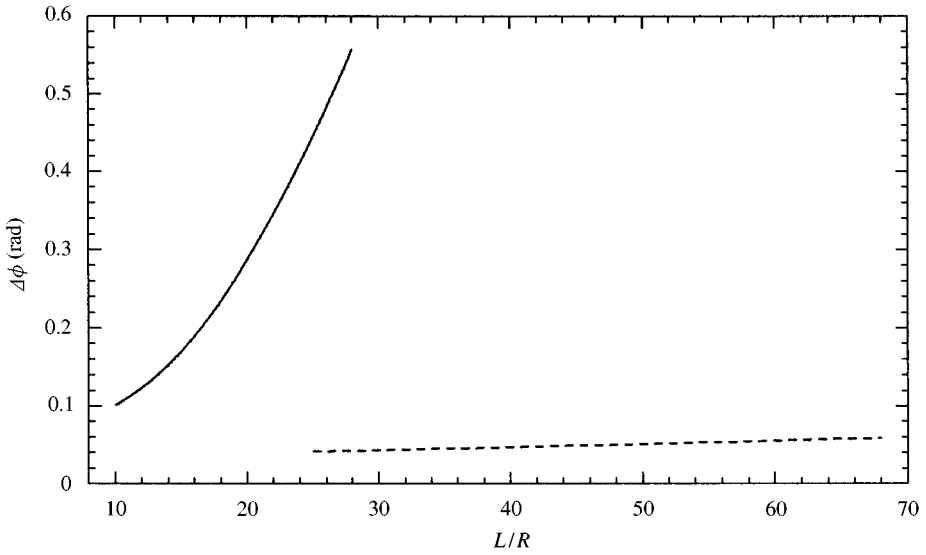
Figure 12. Variation of the phase difference with the tube length ratio for $n = 2$ and 1 ($s/L = 0.5$, other data as in Figure 11): ———, shell-type meter, $n = 2$; - - -, beam-type meter, $n = 1$.
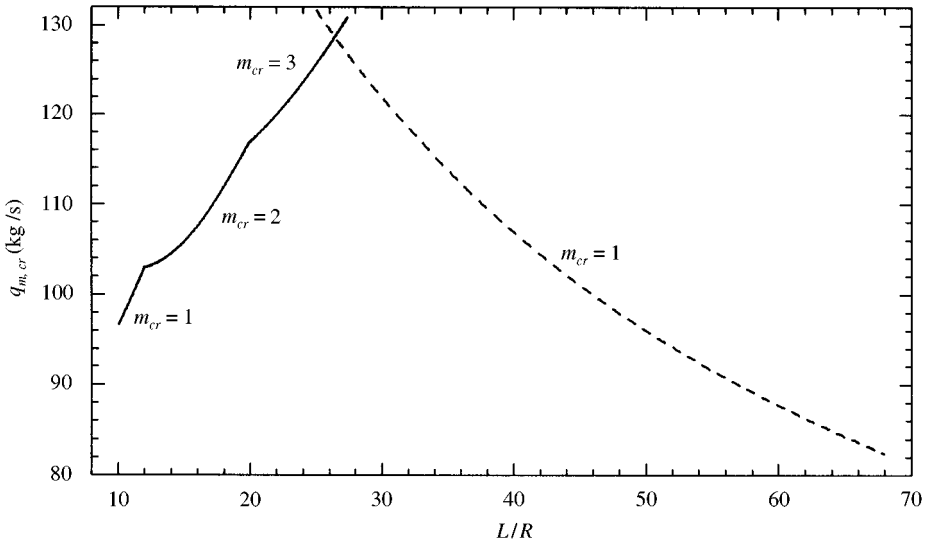

Figure 13. Variation of the critical mass flowrate with the tube length ratio for $n = 2$ and 1 (data as in Figure 11): ———, shell-type meter, $n = 2$; - - -, beam-type meter, $n = 1$.

processing with regard to the noise influence. In addition, the larger phase difference could be used for widening the measuring range or reducing pressure loss.

In section 3, it is shown that approaching the stability boundary gives rise to a dependence of the mass flowrate and fluid density measurement. For this reason, Figure 13 shows the variation of the critical mass flowrate for both meters. The beam-type meter is associated with one axial half-wave at the critical flowrate
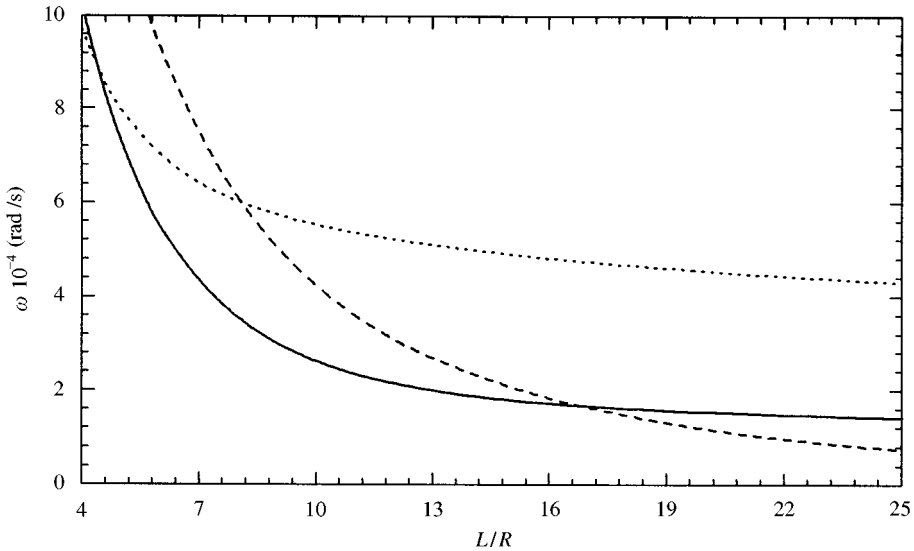
Figure 14. Variation of the natural frequency with the tube length ratio for three values of circumferential wave-number (data as in Figure 11): ——, $n = 2$; - - -, $n = 1$; · · · ·, $n = 3$.

$(m_{cr} = 1)$. The shell-type meter could also result in the higher values of m_{cr}; boundaries between neighbouring m_{cr} are visible as discontinuities in the curve in Figure 13. A weak point of the beam-type meter is its critical flow decreasing in the direction of increasing sensitivity.

Finally, a look at the nature of the lowest natural frequencies of the system under research (Figure 14). For a sufficiently short, thin shell, the natural frequencies can be similar (and also coincide) for different circumferential modes n. This could make controlling the working mode of the meter more difficult. However, the position of the exciters shown in Figure 2 and their counter-phase action prevent the existence of the modes with odd circumferential waves ($n = 1, 3, 5, ...$) and even axial half-waves ($m = 2, 4, 6, ...$), where are also the most "dangerous" modes for the shell-type Coriois meter.

5. CONCLUSION

This paper presents the theoretical analyses of the shell-type Coriolis flowmeter primary part, which is the straight measuring tube conveying fluid to be measured. The measuring principle of the shell-type Coriolis meter is identical to that of the beam-type. The Coriolis force, caused by fluid flow, changes the fundamental mode shape of the measuring tube. The phase difference between the radial motion of two symmetrically positioned measuring points is linearly dependent on the mass flowrate. Using the time difference, independence of the fluid density is assured. Due to the fluid added mass effect on the system natural frequency, the Coriolis meter is used for fluid density measurement, too.

However, it was found that the shell-type Coriolis meter has some significant advantages over the beam-type one. A comparison was made using measuring

tubes with the same internal pressure loss. In general, the shell-type meter provides an essentially larger natural frequency and phase difference. It also gives an assurance of a sufficient distance from the stability boundary.

The mathematical model used in this paper contains some limitations in comparison with the actual realization of the Coriolis flowmeters. The model describes only the mechanical part of the meter without the electronics. However, there are also other parameters not included: the damping of the vibrating system, the effects of the local exciting force, added masses of the exciter and motion sensors, elastic boundary conditions, etc.

REFERENCES

1. G. Sultan and J. Hemp 1989 *Journal of Sound and Vibration* **132**, 473–489. Modelling of the Coriolis mass flowmeter.
2. H. Raszillier and F. Durst 1991 *Archive of Applied Mechanics* **61**, 192–214. Coriolis-effect in mass flow metering.
3. H. Raszillier and V. Raszillier 1991 *Flow Measurement and Instrumentation* **2**, 180–184. Dimensional and symmetry analysis of Coriolis mass flowmeters.
4. H. Raszillier, N. Alleborn and F. Durst 1993 *Archive of Applied Mechanics* **63**, 219–227. Mode mixing in Coriolis flowmeters.
5. H. Raszillier, N. Alleborn and F. Durst 1994 *Archive of Applied Mechanics* **64**, 373–382. Effect of a concentrated mass on Coriolis flowmetering.
6. U. Lange, A. Levient, T. Pankratz and H. Raszillier 1994 *Flow Measurement and Instrumentation* **5**, 255–262. Effect of detector masses on calibration of Coriolis flowmeters.
7. J. Hemp 1988 *Quarterly Journal of Mechanics and Applied Mathematics* **41**, 503–520. Flowmeters and reciprocity.
8. J. Hemp 1994 *Flow Measurement and Instrumentation* **5**, 247–253. The weight vector theory of Coriolis mass flowmeters.
9. J. Hemp and L. A. Hendry 1995 *Flow Measurement and Instrumentation* **6**, 259–264. The weight vector theory of Coriolis mass flowmeters—Part 2. Boundary source of secondary vibration.
10. J. Kutin and I. Bajsić 1997 *XIV IMEKO World Congress* (*Vol. VI*), 87–92. Tampere: Finnish Society of Automation. Modelling of the shell-type Coriolis mass flowmeter.
11. J. Kutin and I. Bajsić 1997 *Kuhljevi dnevi '97*, 225–232. Mokrice: Slovene Society of Mechanics. Measuring effect of the shell-type Coriolis mass flowmeter (in Slovene).
12. R. D. Blevins 1994 *Flow-induced Vibration*. Malabar: Krieger, second edition.
13. S.-S. Chen 1987 *Flow-induced Vibration of Circular Cylindrical Structures*. Washington: Hemisphere.
14. E. Naudascher and D. Rockwell 1994 *Flow-induced Vibrations*: *An Engineering Guide*. Rotterdam: A.A. Balkema.
15. W. Flügge 1966 *Stresses in Shells*. Berlin: Springer, third printing.
16. H. Kraus 1967 *Thin Elastic Shells*. New York: Wiley.
17. S.-I Pai 1959 *Introduction to the Theory of Compressible Flow*. Princeton: Van Nostrand.
18. M. P. Paidoussis and J.-P. Denise 1972 *Journal of Sound and Vibration* **20**, 9–26. Flutter of thin cylindrical shells conveying fluid.
19. D. S. Weaver and B. Myklatun 1973 *Journal of Sound and Vibration* **31**, 399–410. On the stability of thin pipes with an internal flow.

20. L. K. SHAYO and H. ELLEN 1974 *Journal of Sound and Vibration* **37**, 535–545. The stability of finite length circular cross-section pipes conveying inviscid fluid.
21. Y. MATSUZAKI and Y. C. FUNG 1977 *Journal of Sound and Vibration* **54**, 317–330. Unsteady fluid dynamic forces on a simply-supported circular cylinder of finite length conveying a flow, with applications to stability analysis.
22. R. D. BLEVINS 1984 *Applied Fluid Dynamics Handbook*. Malabar: Krieger.

APPENDIX

According to the symbolic form of Flügge's equations (1) the linear differential operators can be expressed as

$$\beta L_{11} = \frac{\partial^2}{\partial \xi^2} + \frac{1-\mu}{2}(1+k)\frac{\partial^2}{\partial \theta^2}, \quad \beta L_{12} = \beta L_{21} = \frac{1+\mu}{2}\frac{\partial^2}{\partial \xi \, \partial \theta},$$

$$\beta L_{13} = \beta L_{31} = \mu \frac{\partial}{\partial \xi} + k\left(\frac{1-\mu}{2}\frac{\partial^3}{\partial \xi \, \partial \theta^2} - \frac{\partial^3}{\partial \xi^3}\right), \quad \beta L_{22} = \frac{1-\mu}{2}(1+3k)\frac{\partial^2}{\partial \xi^2} + \frac{\partial^2}{\partial \theta^2},$$

$$\beta L_{23} = \beta L_{32} = \frac{\partial}{\partial \theta} - \frac{3-\mu}{2}k\frac{\partial^3}{\partial \xi^2 \, \partial \theta}, \quad \beta L_{33} = 1 + k + 2k\frac{\partial^2}{\partial \theta^2} + k\left(\frac{\partial^2}{\partial \xi^2} + \frac{\partial^2}{\partial \theta^2}\right)^2,$$

where μ is the Poisson ratio, $\beta = \rho_t(1-\mu^2)R^2/E$, $k = h^2/(12R^2)$ and $\xi = x/R$.